IJNRD.ORG ISSN : 2456-4184
INTERNATIONAL JOURNAL OF NOVEL RESEARCH AND DEVELOPMENT (IJNRD) | IJNRD.ORG
An International Open Access, Peer-reviewed, Refereed Journal

# Performance Analysis of Micro Grid Connected Wind Driven DFIG, DG and Solar PV Array by Employing Fuzzy Logic Controller for Optimal Fuel Consumption

**M.Sarath Babu, PG student in Sir C R Reddy College of Engineering, sarathcrrpoly@gmail.com**

**Mrs T.Deepti Prasana, Asst Professor, Department of EEE, Sir C R Reddy College of Engineering,tata.deepti@gmail.com Engineering,tata.deepti@gmail.com**

**N Venkata Ramana, Lecturer, Department of EEE, Sir C R Reddy polytechnic,ramanacrrpoly@gmail.com**

**Abstract:**

The main objective of this project is to minimize the fuel consumption of DG. Diesel generators (DGs) are very popular for the decentralized power generation as well as backup power in the urban housing society. DGs suffer from the higher running cost along with noise and air pollution. The running cost is dependent on amount of fuel consumption based on the power generation. This cost is minimized by installing renewable energy (RE) sources such as wind, solar and biomass etc. Moreover, RE based power sources are pollution free and abundant in nature. Among RE sources, wind and solar are considered to be more popular because of their reduced cost and technological advancements. Therefore to overcome the electricity utilization losses, this paper proposes a micro grid i.e. powered by two renewable energy sources namely wind energy using doubly fed induction generator (DFIG) and solar photo voltaic (PV) array. The simulation results for various scenarios such as varying wind speeds, varying insolation, effect of load variation on a bidirectional converter and unbalanced nonlinear load connected at point of common coupling (PCC) can be evaluated by using Matlab/Simulink Software. In this Project Micro grid performance is analysed based on Wind Driven DFIG, DG and Solar PV Array for Optimal Fuel Consumption in the controlling topology PI Controllers are used. This PI Controllers will have high starting overshoot, sensitivity to controller gains and sluggish response to sudden disturbances. So, to overcome this issue Fuzzy Logic Controllers are going to implement in the place of PI Controllers. Fuzzy logic controllers are easy to implement and have good speed response of the system. Results of this proposed method can be evaluated by using Matlab/Simulink Software.

**Keywords**— Wind Turbine, doubly fed induction generator (DFIG), diesel generator, solar photovoltaic array, bidirectional buck/boost DC-DC converter, battery energy storage, power quality, Fuzzy Logic Controller.

## INTRODUCTION:

Diesel generators (DGs) are very popular for the decentralized power generation as well as backup power in the urban housing society for the following reasons.

- DGs are portable and dispatchable.
- They are of lower capital cost.

- DGs maintenance is easier.
- They have higher conversion efficiency as compared to other sources of energy resulting in low specific greenhouse gas emission.

For the above reasons, they are widely used for the power distribution of islands, commercial and military ships etc. However, DGs suffer from the higher running cost along with noise and air pollution. The running cost is dependent on amount of fuel consumption based on the power generation. This cost is minimized by installing renewable energy (RE) sources such as wind, solar and biomass etc. Moreover, RE based power sources are pollution free and abundant in nature. Among RE sources, wind and solar are considered to be more popular because of their reduced cost and technological advancements. Wind turbines are mainly categorized as fixed speed and variable speed type. Fixed speed wind turbines have been used earlier due to their simple operating features. However, they suffer with more power loss. Variable speed wind turbines with doubly fed induction generator (DFIG), are dominantly used for wind energy extraction due to its advantages such as reduced converter rating, less acoustic noise, highly energy efficient and low power loss. Substantial literature on DFIG based wind energy conversion system (WECS) both in standalone and grid connected modes is available. In the authors have presented DFIG based WECS operating in standalone with battery energy storage (BES) connected directly at the DC link. Moreover, the comparative performance with and without BES is discussed. In the authors have described an extended active power theory for effective operation of wind turbine coupled DFIG both in balanced and unbalanced grid conditions. Moreover, the DFIG is controlled with only rotor side converter (RSC). Therefore, the topology suffers from the power quality issues especially during harmonic loads. Liu *et* have investigated the influence of phase locked loop parameters and grid strength on the stability of DFIG wind farm in grid connected mode. However, an experimental validation has not been performed. This work presents a microgrid based on wind turbine driven DFIG, DG and solar PV array with BES, in order to minimize the fuel consumption of DG. In this, the DG is designed to deliver the base load requirement of a particular household locality. The main contributions of this study are on the control aspects of the scheme, which are as follows.

- A novel generalized concept is used to compute the reference DG power output for the DG to remain operating in optimal fuel consumption mode.
- The load side converter control (LSC) is designed to control DG along with the power quality issues such as load unbalance compensation, harmonics compensation and reactive power compensation.
- The RSC control is designed to extract maximum power from the wind turbine.
- The BES is connected to the common DC bus of back-back connected VSCs through a bidirectional buck/boost DC-DC converter. It aims to provide path for excess stator power of DFIG. Moreover, a solar PV array is directly connected at DC bus.
- The bidirectional buck/boost DC-DC converter control is designed in a way to extract maximum power from the solar PV array and to control the current through BES.
- A modified perturb and observe (P&O) MPPT algorithm is presented to obtain maximum power from a solar PV array.
- This microgrid configuration is implemented with minimum number of converters, thereby reducing the total system cost and switching losses.
- The DFIG stator currents and DG currents, are maintained balanced and sinusoidal, as per the IEEE 519 standard.

The wind-diesel-solar microgrid with BES is modelled and simulated using Sim Power Systems tool box of MATLAB. The system performance is analyzed for variable wind speeds, variable insolation, effect on buck boost converter at varying loads and unbalanced nonlinear load connected at point of common coupling (PCC). To validate the microgrid operation, tests are performed on a developed prototype in the laboratory.

## CONFIGURATION OF MICROGRID

The schematic configuration of the micro grid is depicted in Fig. 1. It consists of wind turbine, DFIG, DG, solar PV array, BES, bidirectional buck/boost DC-DC converter, RSC, LSC, interfacing inductors, Ä/Y transformer, linear and nonlinear loads, circuit breakers (CB1 & CB2), DC link capacitor and ripple filters etc. This micro grid is designed to deliver a peak load of 7.5 kW for a particular locality. The wind turbine generator and solar PV array are designed to deliver a power of 7.5 kW each. In this scheme, the solar PV array is directly connected to DC link, whereas BES is connected through bidirectional buck/boost DC-DC converter. The DG comprises of a synchronous generator of 4 poles, internal combustion engine of 4 stroke reciprocating type along with automatic voltage regulator (AVR).A 7.5 KVA. DG is selected in line with rated capacity of the wind turbine generator. The design of a wind turbine generator, solar PV array, DG, BES and other components, is carried out based on the literature reported. Moreover, the design parameters of micro grid are given in Appendices. The complete description of control algorithms of RSC and LSC, MPPT algorithm of solar PV array, bidirectional buck/boost DC-DC converter, are given in following subsections.

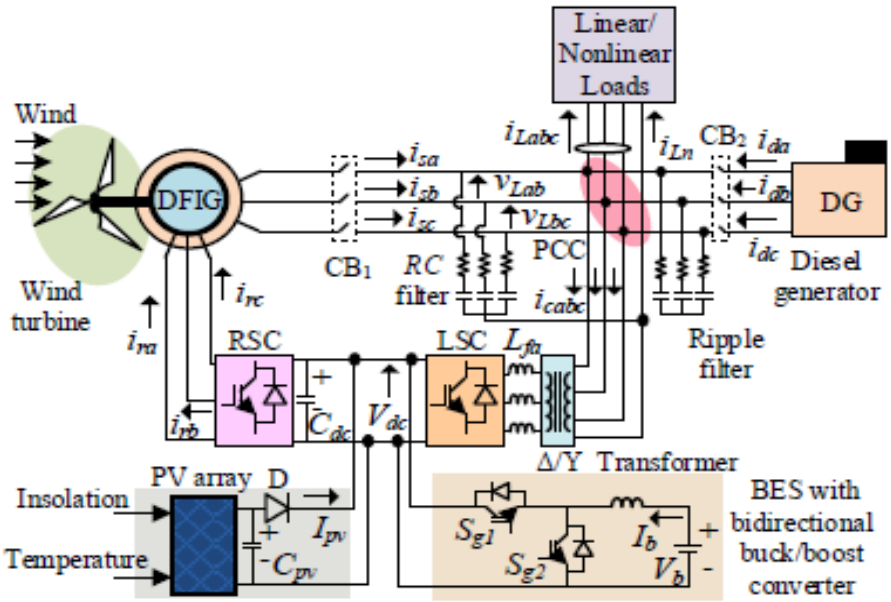


Fig 1 DFIG based micro grid

### Control Algorithm for RSC

The control algorithm of RSC is depicted in Fig. 4 the RSC is used to supply the reactive power requirement of DFIG and also to regulate the speed for achieving MPPT from the wind turbine. The field oriented vector control (FOVC) is used for RSC to generate the switching pulses, as shown in Fig. 4.2. In FOVC, direct axis and quadrature axis components of rotor currents ($I^*_{dr}$, $I^*_{qr}$) represent reactive and active

components, respectively. The $I^*_{dr}$ is corresponding to no load magnetizing current ($I_{rms0}$) of DFIG, which is computed as,

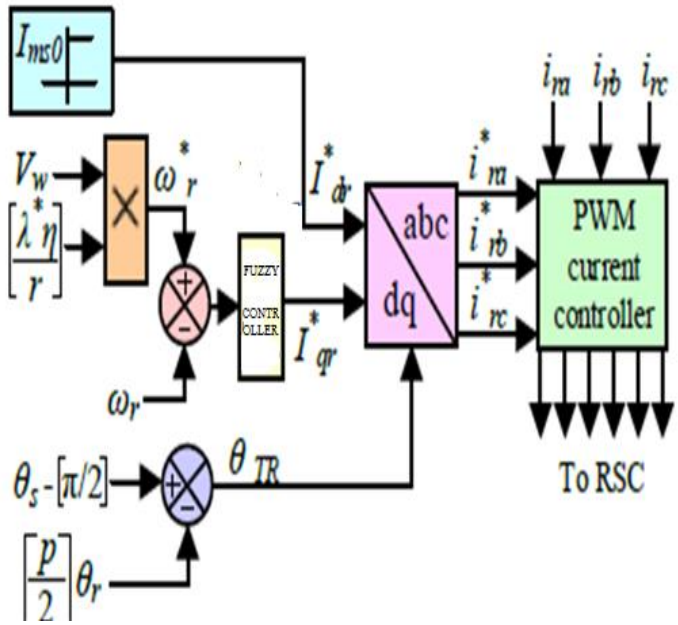


Fig 2 RSC control algorithm

$$I_{ms0} = \frac{\sqrt{2}V_L}{\sqrt{3}X_m} \quad (1)$$

Where $X_m$ denotes the magnetizing reactance of the machine and VL is the line voltage at the machine terminals. The I*qr is estimated by passing the speed error through proportional and integral (PI) controller as depicted in Fig. 4.2 and it is derived as,

$$I^*_{qr(k)} = I^*_{qr(k-1)} + K_{p\omega}(\omega_{err(k)} - \omega_{err(k-1)}) + K_{i\omega}\omega_{err(k)} \quad (2)$$

Where $K_{p\acute{\omega}}$ and $K_{i\acute{\omega}}$ represent proportional and integral constants of PI speed controller, respectively. The $W_{err\,(k)}$ and $W_{err\,(k-1)}$ denote speed error at kth and (k-1) th instants, respectively.

The $W_{err\,(k)}$, is obtained as,

$$\omega_{err(k)} = \omega^*_{r(k)} - \omega_{r(k)} \quad (3)$$

Where $\omega^*_{r\,(k)}$ and $\omega_{r\,(k)}$ denote the reference and sensed rotor speed of DFIG at kth instant, respectively.

The reference rotor speed is obtained from the tip speed ratio MPPT control as,

$$\omega^*_r = \eta\lambda^* V_w / r \quad (4)$$

Where $V_W$, $\lambda^*$,$\eta$ and r represent wind speed, optimal tip speed ratio, gear ratio and radius of wind turbine, respectively. The rotor transformation angle ($\Theta_{TR}$) is computed as,

$$\theta_{TR} = \left(\theta_s - \frac{\pi}{2}\right) - \left(p/2\right)\theta_r \quad (5)$$

Where $\theta_s$ is obtained from phase locked loop and $\theta_r$ is computed from the sensed rotor speed as,

$$\theta_r = \int_0^t (\omega_r)dt \quad (6)$$

Finally, reference rotor currents ($i^*_{ra}$, $i^*_{rb}$ and $i^*_{rc}$) are derived from $I^*_{qr}$ and $I^*_{dr}$ using an angle of transformation $\Theta_{TR}$, as depicted in Fig. 4.2. These reference currents along with sensed. Rotor currents ($i_{ra}$, $i_{rb}$ and $i_{rc}$), are applied to pulse width modulation (PWM) controller to produce RSC gating signals.

**Control Algorithm for LSC**

The LSC control algorithm is depicted in Fig. 4.3. The LSC is controlled to achieve the following objectives.

- It maintains the DG and DFIG stator currents sinusoidal and balanced.
- It regulates the DG power within the range of $PD_{min}$ to $PD_{max}$ to achieve optimal fuel consumption. Where $PD_{min}$ and $PD_{max}$ refer to minimum and maximum DG power output in Pu for optimal fuel consumption.

A modified indirect vector control based on voltage oriented reference frame is used to generate the reference currents as shown in Fig.4.3. In this, both DG and DFIG stator currents are added and controlled to extract maximum power from the DFIG and to regulate the DG power within the range for optimal fuel consumption. The d-axis component of LSC is obtained as,

$$I^*_{dg} = I^*_{dd} + I^*_{dw} \tag{7}$$

Where $I^*_{dd}$, $I^*_{dw}$ denote the d-component current of DG and DFIG, respectively. It is noted that the saturation block is placed before the $I^*_{dd}$ component to operate the DG in optimal fuel efficient zone at change in load, as depicted in Fig.4.3.

In this work, a generalized concept is used to calculate the DG power based on state of the BES. The reference DG power in Pu (P*D) is computed as,

$$P^*_D = P_{D\min} + k_1\beta \tag{8}$$

Here the value of β varies from 0 to 1. The minimum value of β is achieved when BES is charged to maximum voltage ($Vb_{max}$) whereas β takes maximum value when BES voltage falls to its minimum value ($Vb_{min}$). The β is of the form as,

$$\beta = \frac{V_{b\max} - V_b}{k_2} \tag{9}$$

In (8) and (9), $k_1$ and $K_2$ represent constant parameters. The value of k1 is selected such that $P^*_D$ attains its maximum limit of optimal fuel consumption as β tends to unity. Moreover, the value of $K_2$ is selected such that the β attains unity at $Vb_{min}$. In this work, the chosen values of $PD_{min}$, $PD_{max}$, $Vb_{max}$, $Vb_{min}$, $k_1$ and $K_2$ are mentioned in Appendices. From (8), the $I^*_{dd}$ is computed as,

$$I^*_{dd} = \left(\sqrt{2/3}\right) \times \left(\frac{P^*_D \times VA_{DG}}{V_L}\right) \tag{10}$$

Where $V_L$ and $VA_{DG}$ represent line voltage at PCC and VA rating of DG, which is chosen as a base value. The $I^*_{dw}$ is computed as,

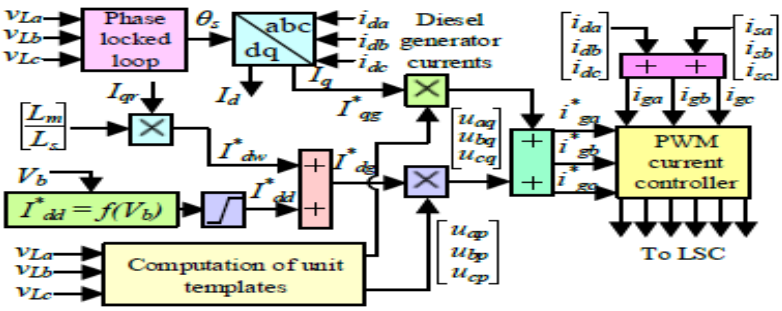


Fig 3 LSC control algorithm

$$I^*_{dw} = \left(\frac{L_m}{L_s}\right) I_{qr} \tag{11}$$

The DG currents ($i_{da}$, $i_{db}$ and $i_{dc}$) are transformed to $I_d$ and $I_q$ using angle of transformation ($\theta_S$), which is obtained from PLL as shown in Fig. 4.3. The q-axis component of LSC current (I*qg) is numerically same as $I_q$ of DG. The $I^*_{dg}$ and $I^*_{qg}$ are multiplied with in-phase and quadrature unit templates, respectively and then added together to generate current references ($i^*_{ga}$, $i^*_{gb}$ and $i^*_{gc}$). The unit templates are obtained from phase voltages ($V_a$, $V_b$ and $V_c$), as shown in Fig. 4.3. Unit templates of in-phase components are obtained as,

$$\left. u_{ap} = \frac{v_a}{V_m}, u_{bp} = \frac{v_b}{V_m}, u_{cp} = \frac{v_c}{V_m} \right\} \tag{12}$$

Where, $V_m$ denotes the peak of phase voltage at PCC, which is computed as,

$$V_m = \{2(v_a^2 + v_b^2 + v_c^2)/3\}^{1/2} \tag{13}$$

The unit templates of quadrature components, are obtained from in-phase components as,

$$\left. \begin{aligned} u_{aq} &= -\frac{u_{bp}}{\sqrt{3}} + \frac{u_{cp}}{\sqrt{3}}, u_{bq} = \frac{\sqrt{3}u_{ap}}{2} + \frac{u_{bp} - u_{cp}}{2\sqrt{3}}, \\ u_{cq} &= -\frac{\sqrt{3}u_{ap}}{2} + \frac{u_{bp} - u_{cp}}{2\sqrt{3}} \end{aligned} \right\} \tag{14}$$

Finally, the generated reference currents and sensed currents ($i_{ga}$, $i_{gb}$ and igc) are applied to PWM controller to produce pulses for LSC, as depicted in Fig.4

**Solar PV Array MPPT Algorithm and Bidirectional Buck/Boost DC-DC Converter Control**

The bidirectional buck or bidirectional boost DC-DC converter is used to regulate the DC link voltage by controlling power flow through the BES. By doing so, the solar MPPT is achieved. In this, a modified perturb and observe (P&O) algorithm is used, which consists of sampling pulse generation (X) and subsequently estimation of reference DC link voltage (V* dc) as depicted in Figs. 4.4-4.5, respectively. Fig. 4.4 illustrates various steps involved in the generation of sampling pulse 'X'. Here, the sampling pulse is a name.

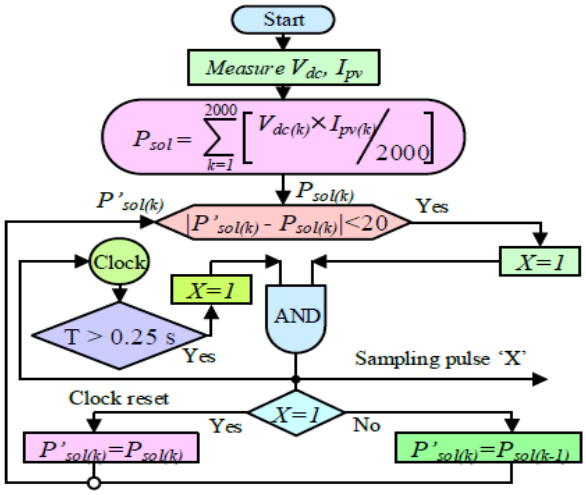


Fig 4 Sampling pulse generation

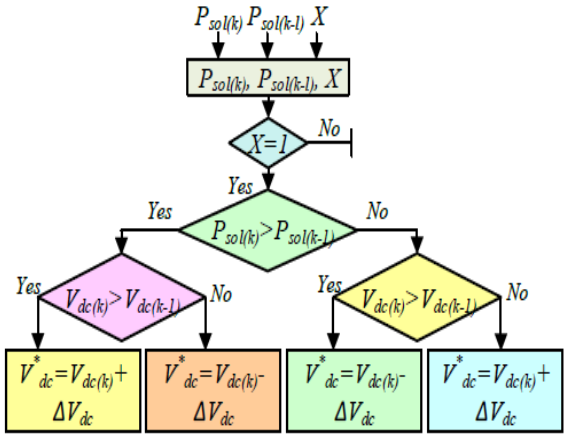


Fig 5 MPPT algorithm of solar PV array

Given to variable 'X'. It varies between digital bits 0 and 1. In Fig. 4.4, the first step is to get the information of DC link voltage or solar PV voltage ($V_{dc}$) and solar PV current ($I_{pv}$) at kth instant and computation of instantaneous solar power. The second step is the determination of running average solar power ($P_{sol}$), which performs the same function as filtering. In case the absolute difference between the running averaged power ($P_{sol}$) and previously sampled power ($P_{sol}$) is less than 20 W combined with minimum time delay of 0.25 s from previous sampling, the control senses that steady state has arrived. On sensing the steady state, the output of the sampling pulse 'X' becomes '1'. The sampling pulse decides the instant of incremental change in reference DC link voltage ($V^*_{dc}$) or solar PV MPPT voltage. The value of $V^*_{dc}$ is updated only if sampling pulse becomes '1'. This is clearly evident from Fig. 4.5 that depicts the modified P&O MPPT algorithm. Once X becomes '1', the MPPT algorithm checks for $P_{sol(k)} > P_{sol(k-1)}$. If it is yes, then it again checks for $V_{dc(k)} > V_{dc(k-1)}$. If it is also yes, then, the new reference DC link voltage becomes $V^*_{dc} = V_{dc\ (k)} + \Delta V_{dc}$.Where $\Delta V_{dc}$ denotes the small incremental change in DC link voltage. The other scenarios are evident from the Fig. 4.5.The bidirectional buck/boost DC-DC converter control, is demonstrated in Fig. 4.6. The outer proportional-integral (PI) controller of the bidirectional buck or bidirectional DC-DC boost converter control, is used to regulate the DC link voltage. Moreover, the output of the outer PI controller is reference battery current ($I^*_b$), as depicted in Fig.4.6. The inner PI controller is used to track the reference battery current. Moreover, the output of the inner PI controller is the duty ratio (R) of the bidirectional buck/boost DC-DC converter. From Fig. 4.6, the reference battery current ($I^*_b$) is obtained as,

$$I^*_{b(k)} = I^*_{b(k-1)} + K_{pb}(V_{de(k)} - V_{de(k-1)}) + K_{ib}V_{de(k)} \qquad (15)$$

Where, error of the DC link voltage at kth instant is

$$V_{de(k)} = V^*_{dc(k)} - V_{dc(k)}$$

Here $V^*_{dc(k)}$ and $V_{dc(k)}$ represent the reference DC link voltage and sensed DC link voltage at kth Instant, respectively. $K_{pb}$ and $K_{ib}$ denote the proportional and integral constants of the outer PI controller. Besides, the duty ratio (R) of the bidirectional DC-DC converter, is computed as,

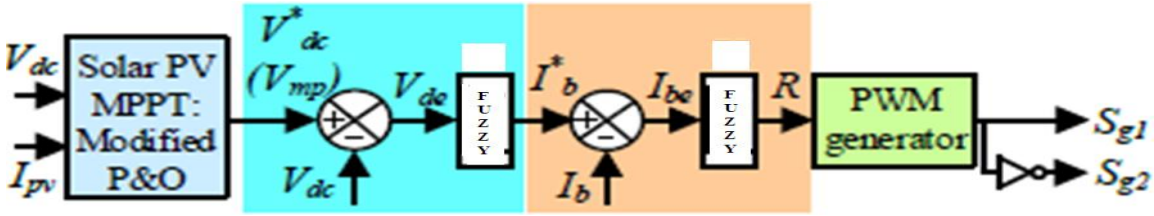


Fig 6 Control of bidirectional buck boost converter

**Integral constants of the outer PI controller:**

Besides, the duty ratio (R) of the bidirectional DC-DC converter, is computed as,

$$R_{(k)} = R_{(k-1)} + K_{pr}(I_{be(k)} - I_{be(k-1)}) + K_{ir} I_{be(k)} \tag{16}$$

Where, error of the battery current at kth instant is

$$I_{be(k)} = I^*_{b(k)} - I_{b(k)}$$

Here $I^*b_{(k)}$ and $I_{b(k)}$ represent the reference battery current and sensed battery current at kth instant, respectively.

The obtained duty ratio (R) is applied to PWM generator to produce pulses for the switches of the bidirectional buck or bidirectional boost converter.

## RESULTS

### I Performance of Bidirectional Buck/Boost Converter at Change in Load:

The performance of bidirectional buck or bidirectional boost DC-DC converter at change in the load is depicted in Figs. 6.1 (a-b). The wind speed and insolation are kept at 7 m/s and 700 W/m2, respectively. Initially a 3-phase balanced load of 2.5 kW is connected at PCC. The DG is delivering 4.84 kW (shown in Fig. 6.1 (b)), which corresponds to the battery bank voltage of 125 V. Moreover, the DFIG and solar PV array powers are 2.013 kW and 4.122 kW, respectively as depicted in Fig. 6.1 (b). Since the total generation is more than the local demand, the remaining power goes to BES through a bidirectional buck/boost DC-DC converter as shown in Fig. 6.1 (a). At $t$ = 3 s, an additional load of 2 kW is connected and again it is disconnected at $t$ = 5.5 s. During this period, it is observed that the power generation from all sources, remains unchanged and the increased load power is met by the BES through LSC. There is minor sag and swell of DC link voltage, however, the solar MPPT is unaffected as seen from $P_{sol}$ waveform. Moreover, the system voltage and frequency are maintained constant, as depicted in Fig. 6.1 (b).

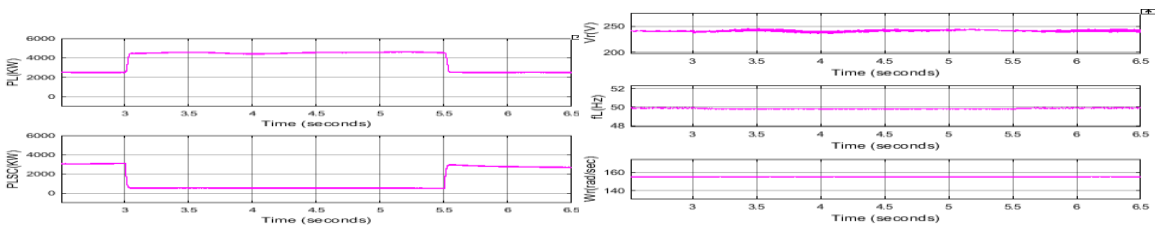

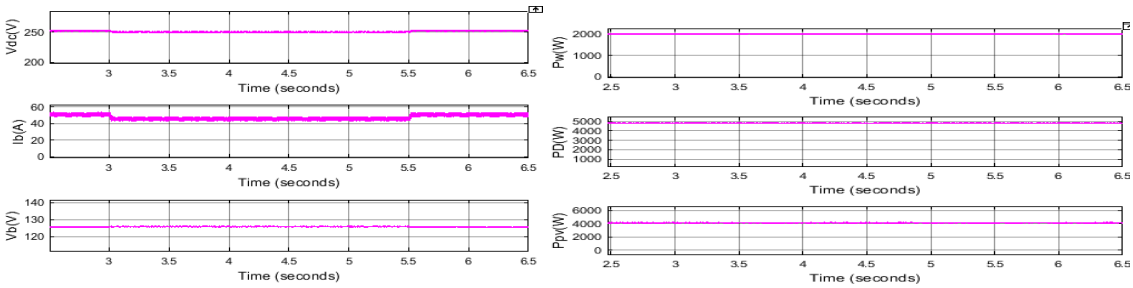


Fig 7 Performance of Bidirectional Buck/Boost Converter at Change in Load

a) $P_l$, $P_{lsc}$, $V_{dc}$, $I_b$ and $V_b$ b) $V_r$, $F_l$, $W_r$, $P_d$, Pw and $P_{sol}$

**II System Performance at Variable Wind Speeds**

The performance of the system at variable wind speeds are depicted in Figs. 8 (a-c). In this, a 3-phase load of 4 kW is connected at PCC and the insolation is kept at 700 W/m2. The DG delivers power of 5.67 kW based on the state of the BES, as depicted in Fig. 8 (b). The pattern of wind speed variation is depicted in Fig. 8 (a). It is observed that the controller regulates the DFIG rotor speed as per wind MPPT algorithm, as depicted in Fig. 8 (a). Moreover, it is observed that the DC link voltage is regulated.

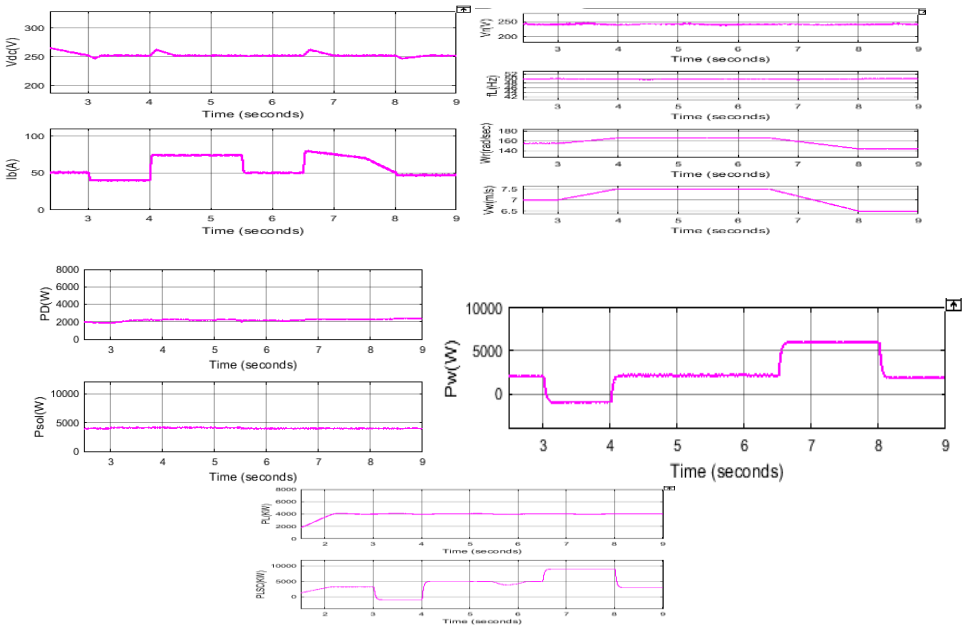


Fig 8 System Performance at Variable Wind Speeds

(a) $V_{dc}$, $I_b$, $P_{sol}$, $P_d$, $P_l$ and $P_{lsc}$ (b) $V_r$, $F_l$, $V_w$, .Wr and $P_w$

**System performance during changeover of DFIG speed from super synchronous to sub synchronous speed region**

The system dynamic response during the transition of DFIG speed from super synchronous to sub synchronous speed region is depicted in Fig. 8 (c). It is observed that wind MPPT is obtained during the variation of wind speed. Moreover, the frequency rotor currents, is changed according to the speed of operation of DFIG.

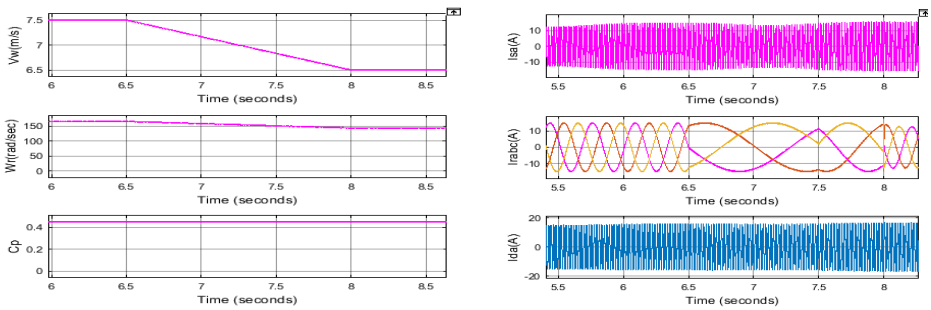


Fig 9 System performance during changeover of DFIG speed from super synchronous to sub synchronous speed region

(c) $V_w$, $W_r$, $C_p$, $I_{sa}$, $I_{rabc}$, $I_{da}$

**III System Performance at Variable Insolation:**

The performance of the system at varying solar radiation is depicted in Figs. 9 (a-b). In this, the wind speed is kept constant at 7 m/s. Moreover, the DG delivers 4.2 kW power based on the battery voltage, as depicted in Fig. 9 (b). In this, a 3-phase linear balanced load of nearly 4 kW is connected at PCC. The insolation of solar PV array is varied from 700 W/m2 to 800 W/m2 at t = 3 s and again it is reduced to 600 W/m2 at t = 5.5 s, as depicted in Fig. 9 (a). The DC link voltage is regulated by the bidirectional DC-DC converter control for achieving the solar MPPT. Moreover, the solar MPPT is manifested by the $P_{sol}$ waveform, as depicted in Fig. 9 (a).

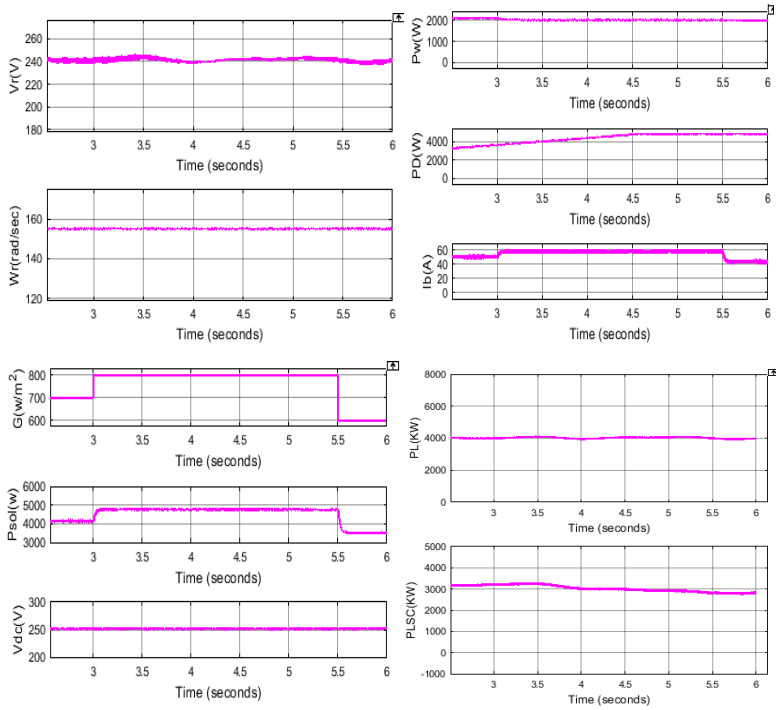


Fig 10 System Performance at Variable Insolation (a) $V_r$, Wr, G, $P_{sol}$ and $V_{dc}$ (b) $I_b$, $P_D$, $P_w$, $P_L$ and $P_{LSC}$.

**System Performance at Unbalanced Nonlinear Load:**

The dynamic performance of the system at unbalanced nonlinear load is depicted in Fig. 10. Initially, a balanced load of 6.7 kW is connected at PCC. It includes a linear load of 0.5 kW and remaining be the nonlinear load, connected on each phase. At t = 2.6 s, a-phase of the load is disconnected and subsequently phase-b, is also disconnected at t = 2.8 s, as depicted in Fig. 10. However, both voltages and currents of DFIG and DG are maintained balanced and follow the IEEE 519 standard. The LSC helps in unbalance and harmonics compensation of the connected load at PCC. The LSC currents and neutral current are also shown in Fig. 10. Moreover, the variation of power at unbalanced nonlinear load is depicted in Fig. 11. Fig. 11 demonstrates waveforms of $V_r$, $V_{dc}$, $I_b$, $P_{sol}$, $P_w$, $P_D$, $P_L$ and $P_{LSC}$. From these results, it is observed that the DC link voltage is regulated and moreover, solar PV and wind MPPT operation is unaffected. The decrease in load power goes to BES through LSC, which is evident from $I_b$, $P_L$ and $P_{LSC}$ waveforms. Moreover, $V_r$ is maintained at constant value.

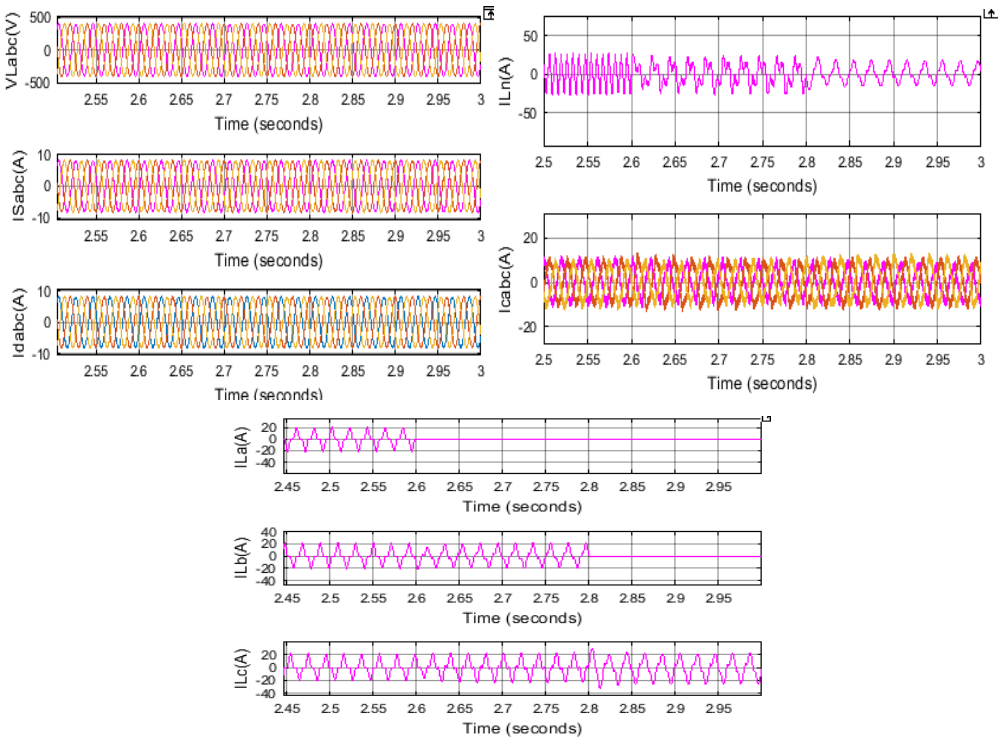


Fig 11 System voltages and currents at unbalanced nonlinear load: $V_{Labc}$, $I_{sabc}$, $I_{dabc}$, $I_{la}$, $I_{lb}$, $I_{lc}$, $I_{ln}$ and $I_{cabc}$.

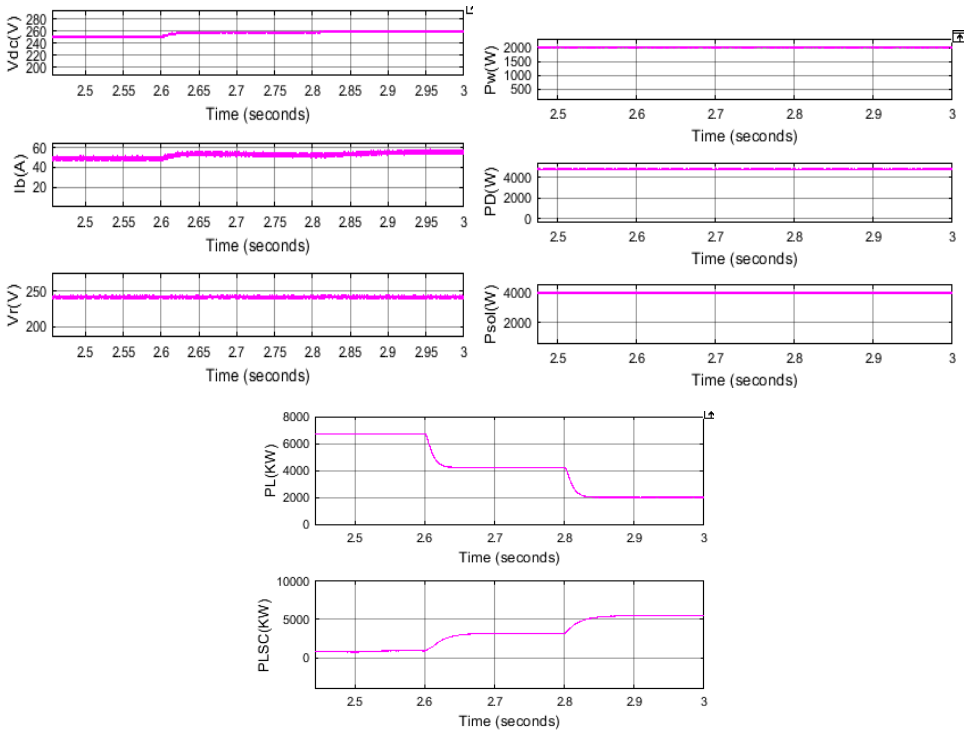


Fig 12 System performance at nonlinear unbalanced load: $V_r$, $V_{dc}$, $I_b$, $P_{sol}$, $P_w$, $P_d$, $P_l$ and $P_{lsc}$

## CONCLUSION

The micro grid based on wind turbine driven DFIG, DG and solar PV array with BES, with minimum number of converters, has been presented. The solar PV array is directly connected to DC link of back-back connected VSCs, whereas BES is connected through a bidirectional buck/boost DC-DC converter. The system has been simulated for various scenarios such as variable wind speeds, variable insolation and unbalanced nonlinear load connected at PCC. Moreover, the performance of bidirectional buck/boost DC-DC converter at change in the load has been investigated.

Simulated results have shown the satisfactory performance of the system to achieve optimal fuel consumption. The DFIG stator voltages, currents and DG currents, are found balanced and sinusoidal, as per the IEEE 519 standard. A prototype has been developed in the laboratory to validate the steady state and dynamic performances of the micro grid. Test results have shown quite good performance under variable wind speeds, linear and nonlinear unbalanced loads and at variable PV insolation.

**REFERENCES**

[1] Ju Liu, Wei Yao, Jinyu Wen, Jiakun Fang, Lin Jiang, Haibo He, and Shijie Cheng, "Impact of power grid strength and PLL parameters on stability of grid-connected DFIG wind farm," IEEE Trans. Sustain. Energy, vol. 11, no. 1, pp. 545-557, Jan. 2020.

[2] S. Puchalapalli and B. Singh, "A single input variable FLC for DFIG-based WPGS in standalone mode," IEEE Trans. Sustainable Energy, vol. 11, no. 2, pp. 595-607, April 2020.

[3] P. Shah, I. Hussain, and B. Singh, "Single-stage SECS interfaced with grid using ISOGI-FLL-based control algorithm," IEEE Trans. Ind. Applicat., vol. 55, no. 1, pp. 701-711, Jan.-Feb. 2019.

[4] S. K. Tiwari, B. Singh, and P. K. Goel, "Control of wind–diesel hybrid system with BESS for optimal operation," IEEE Trans. Ind. Applicat., vol. 55, no. 2, pp. 1863-1872, March-April 2019.

[5] A. Thakallapelli, S. Kamalasadan, K. M. Muttaqi, and M. T. Hagh, "A synchronization control technique for soft connection of doubly fed induction generator based wind turbines to the power grids," IEEE Trans. Ind. Applicat., vol. 55, no. 5, pp. 5277-5288, Sept.-Oct. 2019.

[6] C. Wu and H. Nian, "Stator harmonic currents suppression for DFIG based on feed-forward regulator under distorted grid voltage," IEEE Trans. Power Electron., vol. 33, no. 2, pp. 1211-1224, Feb. 2018.

[7] D. Sun, X. Wang, H. Nian, and Z. Q. Zhu, "A sliding-mode direct power control strategy for DFIG under both balanced and unbalanced grid conditions using extended active power," IEEE Trans. Power Electron., vol. 33, no. 2, pp. 1313-1322, Feb. 2018.

[8] W. Li, P. Chao, X. Liang, J. Ma, D. Xu, and X. Jin, "A practical equivalent method for DFIG wind farms," IEEE Trans. Sustain. Energy, vol. 9, no. 2, pp. 610-620, April 2018.

[9] A. K. Singh, I. Hussain, and B. Singh, "Double-stage three-phase grid-integrated solar PV system with fast zero attracting normalized least mean fourth based adaptive control," IEEE Trans. Ind. Electron., vol. 65, no. 5, pp. 3921-3931, May 2018.

[10] N. Nguyen-Hong, H. Nguyen-Duc, and Y. Nakanishi, "Optimal sizing of energy storage devices in isolated wind-diesel systems considering load growth uncertainty," IEEE Trans. Ind. Applicat., vol. 54, no. 3, pp. 1983-1991, May-June 2018.

[11] J. Jo, H. An, and H. Cha, "Stability improvement of current control by voltage feedforward considering a large synchronous inductance of a diesel generator," IEEE Trans. Ind. Applicat., vol. 54, no. 5, pp. 5134-5142, Sept.-Oct. 2018.

[12] Y. Zhang, A. M. Melin, S. M. Djouadi, M. M. Olama and K. Tomsovic, "Provision for guaranteed inertial response in diesel-wind systems via model reference control," IEEE Trans. Power Systems, vol. 33, no. 6, pp. 6557-6568, Nov. 2018.

[13] J. Knudsen, J. D. Bendtsen, P. Andersen, K. K. Madsen, and C. H. Sterregaard, "Supervisory control implementation o/n diesel-driven generator sets," IEEE Trans. Ind. Electron., vol. 65, no. 12, pp. 9698-9705, Dec. 2018-